Received: 7 January 2019 | Revised: 22 March 2019 | Accepted: 30 March 2019

DOI: 10.1002/poc.3968

RESEARCH ARTICLE

WILEY Journal of Physical Organic Chemistry

4-(4-Bromophenyl)thiazol-2-amine: Crystal structure determination, DFT calculations, visualizing intermolecular interactions using Hirshfeld surface analysis, and DNA binding studies

Pervaiz A. Channar[1] | Nasima Arshad[2] | Fayaz A. Larik[1] | Shahid I. Farooqi[2] | Aamer Saeed[1] | Tuncer Hökelek[3] | Bakhtawar Batool[1] | Rabail Ujan[4] | Hafiz Saqib Ali[5] | Ulrich Flörke[6]

[1]Department of Chemistry, Quaid-i-Azam University, Islamabad, Pakistan

[2]Department of Chemistry, Allama Iqbal Open University, Islamabad, Pakistan

[3]Department of Physics, Faculty of Engineering, Hacettepe University, Beytepe-Ankara, Turkey

[4]Dr. M. A. Kazi Institute of Chemistry, University of Sindh, Jamshoro, Pakistan

[5]School of Chemistry, The University of Manchester, Manchester, UK

[6]Department Chemie, Fakultätfür Naturwissenschaften, Universität Paderborn, Paderborn, Germany

Correspondence

Nasima Arshad, PhD, Department of Chemistry, Allama Iqbal Open University, 44000 Islamabad, Pakistan.
Email: nasimaa2006@yahoo.com; nasima.arshad@aiou.edu.pk

Aamer Saeed, PhD, Department of Chemistry, Quaid-i-Azam University, 45320 Islamabad, Pakistan.
Email: aamersaeed@yahoo.com

Abstract

2-Aminothiazole is a valuable synthon in organic synthesis and an important structural unit of pharmaceutically active drugs. It is accessible via several synthetic routes. In the current account, compound **4** {4-(4-bromophenyl) thiazol-2-amine} was synthesized by employing a recently reported procedure of Gabriel synthesis using Lawesson reagent. The title compound was characterized through spectro-elemental analytical data, and its crystal structure was determined by single-crystal X-ray diffraction. The torsion angles, bond lengths, and bond strengths between the planes of the thiazole and phenyl rings were optimized by theoretical calculations by applying the B3LYP/6-311++G(d,p) level for the purpose of investigating the conformational effects on the stabilization of the crystal packing. HOMO-LUMO analysis, vibrational analysis, and thermodynamic parameters were also investigated. A detailed analysis of the intermolecular interactions of thiazole moiety bearing the amino and bromophenyl ring has been performed based on the Hirshfeld surfaces and their associated two-dimensional fingerprint plots. The relative contributions of the main intermolecular contacts as well as the enrichment ratios derived from the Hirshfeld surface analysis establish the 2-aminothiazole synthon to be a molecule of great interest. DNA binding studies pointed towards anticancer potency of the synthesized compound via reversible binding.

KEYWORDS

2-aminothiazole, DFT calculations, DNA binding, Hirshfeld surface analysis, X-ray crystal analysis

1 | INTRODUCTION

Thiazole nucleus has been known for a long time. Earlier work on benzothiazole has been reported by Hoffman in 1879.[1] However, a systematic study on the thiazole moiety of several derivatives was reported in 1887 from Hantzsch laboratory. Since then, the chemistry of thiazole has enjoyed unprecedented attention and has

found multitudinous aspects such as methods of synthesis, physical properties, structure and reactivity, reaction mechanism, and industrial and biological applications.[2–5] The structural insights of thiazole units reveal that it possesses aromatic character, having resonating double bonds and furthermore its chemical and physical properties resemble with pyridine unit. However, thiazole is the weaker base ($pKa = 2.52$) than pyridine ($pKa = 5.20$), but 2-aminothiazole ($pKa = 5.28$) is more basic than simple thiazole and pyridine.

Thiazole motif is a vital component of many commercial drugs. Dasatinib (antineoplastic agents),[6] ritonavir (anti-HIV drug),[7] ravuconazole (antifungal agent),[8] fanetizole (anti-inflammatory agents),[9] nizatidine (anti-ulcer agent),[10] and thiamethoxam (insecticide)[11,12] are few examples of thiazole bearing products (Figure 1). 1,3-Thiazole units have achieved an enormous amount of success in the design of mesogenic liquid crystalline materials due to their abilities to improve or modify the mesogenic behaviour and physical properties such as dielectric anisotropy, polarizability, viscosity, elastic constants, and luminescence. 1,3-Thiazole displays a linear structure, and hence, it has the aptitude to exhibit broad mesophases and polymorphism.[13,14]

Formidable goals have been achieved in the synthetic methodologies of heterocycles since the beginning of the second half of the last century. 2-Aminothiazoles can be easily accessed by various approaches such as by using thiourea and ketones, thiourea and NBS (*N*-bromosuccinimide), thiourea and oxidizing agents, and alpha-haloketones. 1,4-Dicarbonyl compounds are widely considered precursors for the synthesis of organosulfur compounds. The thionation can be performed with a variety of reagents, including phosphorus pentasulfide,[15,16] hydrogen sulfide,[17,18] thiophosphoryl chloride,[19] bis(trimethylsilyl)sulfide[20] and rhodanine. In 1956, Lawesson reagent (LR) was introduced as an efficient and high-yielding versatile thionating reagent. 1,3-Thiazoles can be synthesized by using LR, and a plethora of literature depicts the extensive use of LR in the synthesis of natural and unnatural organosulfur compounds.[21–24]

In this current account, we envision to synthesize 2-aminothiazole molecule using LR as an effective thionating reagent. Moreover, the chemical reactivity, surface analysis, structural properties, and DNA binding of the title compound were also explored.

2 | EXPERIMENTAL

2.1 | Chemical and reagents

All chemical and reagents used in synthesis and DNA binding experiments were commercially available and used as received. Solvents (reagent grade) were dried and redistilled prior to being used. Autoclave water and apparatus were used during DNA extraction.

2.2 | Instrumentations

Melting points were recorded using a digital Gallenkamp (SANYO) model MPD.BM 3.5 apparatus and are uncorrected. ^{1}H and ^{13}C NMR spectra were determined at 300 MHz using a Bruker AM-300 spectrophotometer. FT-IR spectra were recorded on a Bio-Rad-Excalibur Series Mode FTS 3000 MX spectrophotometer. Elemental analyses were conducted using a LECO-183 CHNS analyser. Thin layer chromatography (TLC) was conducted on 0.25-mm silica gel plates (60 F254, Merck). Visualization of chromatograms was made with UV at 365 and 254 nm. R_f values were calculated using a solvent system of petroleum ether: ethyl acetate in 4:1

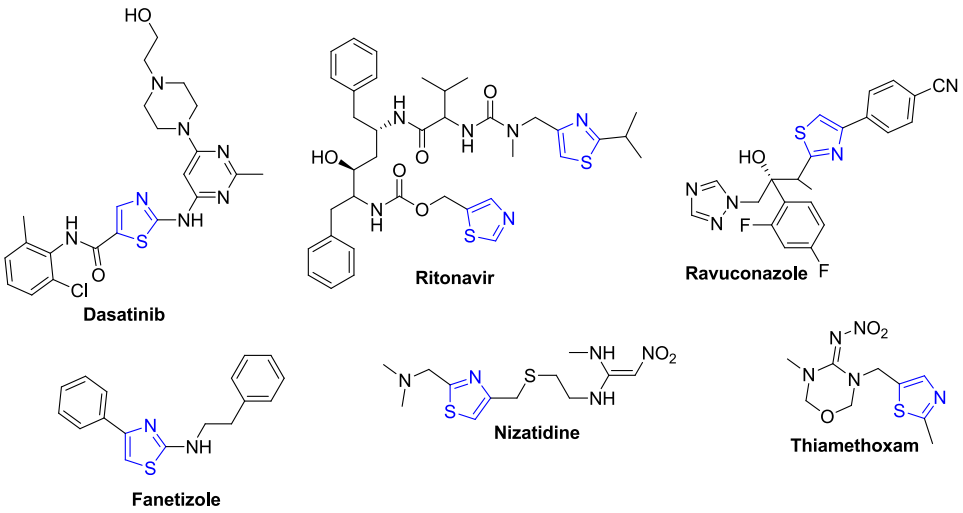

FIGURE 1 Examples of thiazole bearing drugs

ratio. Shimadzu 1800 spectrophotometer equipped with temperature controller device was used for DNA binding experiment, while Schott Gerate viscometer (automated, Model; AVS 310) was used to measure the viscosity of DNA without and in the presence of varying compound concentrations.

2.3 | Synthesis of 4-(4-bromophenyl) thiazol-2-amine

To the stirring solution of 2-bromo-1-(4-bromophenyl) ethanone (0.5 g, 2.016 mmol), in the mixture of tetrahydrofuran and ethanol (10 mL), urea (2.016 mmol) was added with anhydrous potassium carbonate and a catalytic amount of potassium iodide. The system was heated under reflux for 6 to 7 hours. The solid product (2-(4-bromophenyl)-2-oxoethyl) urea **3** was obtained. After filtration, re-crystallization of the product was made with ethanol—chloroform mixture. The compound **3** was treated with LR using 3 mmol of compound **3** in 3 mL of toluene with 3 mmol of LR, and the resulting mixture was heated for 3.5 hours with stirring. On completion, the reaction mixture was cooled to ambient temperature and then concentrated in vacuum. A yellow solid of 4-(4-bromophenyl)thiazol-2-amine **4** was obtained in good yield. The final compound was further recrystallized from ethanol/water (1/1), and the slow evaporation yielded small crystals suitable for X-ray analysis.

2.4 | Characterization data

Yield:80%: M. P 188°C; R_f: 0.67; Petroleum ether: ethyl acetate (6:4) IR; (KBr, cm^{-1}): 3375 (NH_2), 3117 (sp^2CH), 1624 (C=N), 1568 (Ar-C=C), ^1H NMR (300 MHz, DMSO-d_6): δ (ppm): 7.31 (s, 1H, thiazole H), 6.12 (s, 2H, NH_2), 6.71-7.20 (m, 4H Ar-H) ^{13}C NMR (75 MHz, DMSO-d_6): δ (ppm): 174.4, 153.0, 136.6, 134.8, 129.6, 124.4, 108.3, Anal. Calcd. for $C_9H_7BrN_2S$: C, 42.37; H, 2.77; N, 10.98; S, 12.57. found: C, 42.39; H, 2.79; N, 10.96; S, 12.58.

2.5 | X-ray crystallography and structure refinement

Crystallographic data were recorded on a Bruker AXS SMART APEX CCD area-detector diffractometer using Mo K_α radiation ($\lambda = 0.71073$ Å) at $T = 130$ K. Absorption correction by multiscan (Bruker, 2005) was applied.[25] The structure was solved by direct methods and refined by full-matrix least squares against F^2 using all data.[26] All non-H atoms were refined anisotropically. Atoms H1 and H2 (for OH_2) were located in a difference Fourier map and refined freely. The N- and C-bound H atoms were positioned geometrically, with N–H = 0.88 Å (for NH and NH_2) and C–H = 0.95 Å for aromatic H atoms, and constrained to ride on their parent atoms with $U_{iso}(H) = 1.2 \times U_{eq}$ (N, C). Full crystallographic data for compound have been deposited with the Cambridge Crystallographic Data Centre (CCDC 1871549).

2.6 | Theoretical calculations

2.6.1 | DFT calculations

All quantum chemical calculations were performed with the GAUSSIAN 09 program package.[27] The initial molecular structures of the title compound were taken from the X-ray crystallographic data. Then, the geometry optimization of the title compound by density functional theory (DFT) was carried using Becke three-parameter hybrid functional combined with the Lee-Yang-Parr correlation functional (B3LYP) with the 6-311++G(d,p) basis set.[28] The vibrational frequencies and thermodynamic parameters were also calculated for the optimized structure at the same level of theory in the gas phase. Since DFT-calculated harmonic vibrational frequencies are usually larger than those observed experimentally, a frequency scaling factor was employed for the vibrational analysis.

2.6.2 | Hirshfeld surface calculations

Crystal Explorer program 17.5 was employed to carry out the Hirshfeld surface (HS) analyses.[29] The structural input file was obtained in the CIF format. HS distance from the nearest nucleus inside and outside the surface was measured and represented by d_i and d_e, respectively, while a normalized contact distance was represented as d_{norm}. White, red and blue colours have been selected for the visualization of d_{norm}.

2.7 | DNA binding experiments

Using Falcon method, double-strand (ds-) DNA was extracted from calf thymus gland and checked for its purity by measuring absorbance at 260 and 280 nm. A_{260}/A_{280} was evaluated 1.86, which showed that the absorbance ratio was satisfactory to assure the DNA purity.[30] The concentration of stock DNA was evaluated at λ_{260} by using the value of the molar extinction coefficient (ε_{260} = 6600 $cm^{-1}M^{-1}$) in Beer law. The stock concentration of the synthesized compound was prepared in 1:1 ethanol: water mixture. For DNA binding

experiments concentration of synthesized compound was optimized to 1.25×10^{-4}M and kept constant while adding DNA from 10 to 60μM under physiological temperature (37°C). Conversely, in viscosity experiments, DNA concentration was kept constant to 1.45×10^{-5}M and compound was added gradually in its increasing concentration from 10 to 90μM.

3 | RESULTS AND DISCUSSION

3.1 | Synthesis

Thiazole containing scaffold was synthesized by following a well-established protocol.[31] In the first step, the nucleophilic substitution reaction was performed by using **1** and **2** to obtain **3**. The latter was subjected to LR under anhydrous conditions to obtain the desired product **4** in excellent yield (Scheme 1). The mechanism for Gabriel cyclization reaction is presented as Scheme S1.[22]

3.2 | Characterization

Synthesized compound was fully characterized by ^{1}H and ^{13}C NMR. In proton NMR, the existence of the thiazole moiety was confirmed by the two proton singlets lying in the aromatic region due to being attached with sp^2 carbon and sulfur and nitrogen electronegative elements. ^{13}C NMR also confirmed the formation of thiazole moiety. Quaternary carbon of thiazole ring, which is directly attached to nitrogen, appeared around 173 ppm, while the ipso carbons appeared at high ppm values and that can also be justified from the height of signal. The carbons appeared around 140 to 120 ppm values indicated their aromatic nature.

3.3 | Crystal structure description

The molecular structure along with the atom-numbering scheme is depicted in Figure 2. The single crystal X-ray structure determination of the title compound confirmed the assignment of its structure from spectroscopic data. The experimental details including the crystal data, data collection, and refinement are summarized in Table 1.

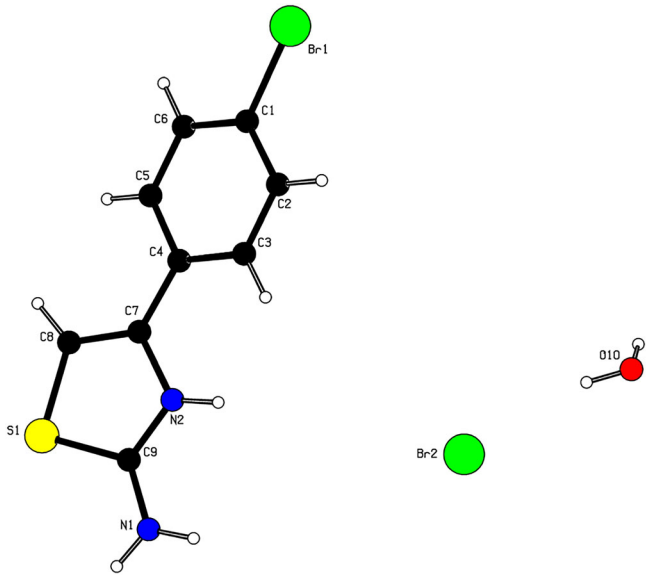

FIGURE 2 The molecular structure of the title compound, with the atom-numbering scheme for the asymmetric unit

The hydrogen bond geometry and the selected interatomic distances are given in Tables 2 and 3, while the selected bond lengths, bond angles together with the torsion angles are provided in Table S1.

The asymmetric unit contains one ligand molecule, one uncoordinated water molecule, and one uncoordinated Br atom. The planar benzene [A (C1-C6)] and thiazole [B (S1/N2/C7-C9)] rings are oriented at a dihedral angle of A/B = 14.82(3)°. Thus, the molecule is nonplanar as a whole. The uncoordinated water molecule is bonded to the uncoordinated Br atom through the intramolecular O_W–H_W···$Br_{unccord}$ (W = water, uncoord = uncoordinated) hydrogen bond (Table 3). In the crystal structure, a significant π···π interaction between the benzene [A (C1-C6)] and thiazole [B (S1/N2/C7-C9)] rings of the adjacent molecules with an intercentroid distance of 3.610(2) Å was observed. On the other hand, there are intermolecular N–H_{Thz}···$Br_{unccord}$, N–H_{Thz}···O_W, C–H···O_W and O_W–H_W···$Br_{unccord}$ (Thz = thiazole) hydrogen bonds (Table 3 and Figure 3).

The π···π interactions and the hydrogen bonds link the molecules into a three-dimensional supramolecular structure. Hydrogen bonding and van der Waals contacts are the dominant interactions in the crystal packing.

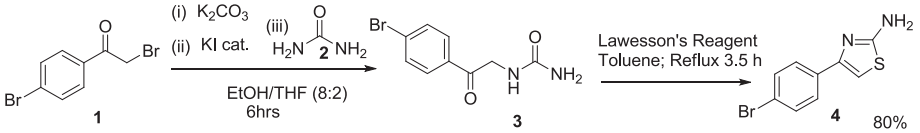

SCHEME 1 Gabriel synthesis of 1,3-thiazole through thionation with Lawesson reagent

TABLE 1 Crystallography data for the title compound

Empirical formula	$C_9H_8BrN_2S{\cdot}Br\ H_2O$
Formula weight	354.07
Temperature	130 K
Wavelength	0.71073 Å
Crystal system	Monoclinic
Space group	P 2_1/c
Unit cell dimensions	a = 13.007(2)Å β = 109.5326(3)° b = 9.6097(17) Å c = 9.9436(17) Å
Volume	1171.1(4) $Å^3$
Z	4
Density (calculated)	2.008 mg m^{-3}
Absorbtioncocfficient	7.08 mm^{-1}
F (000)	688
Crystal size	0.32 × 0.17 × 0.04 mm^3
Θ range for data collection	2.7-28.3°
Index ranges	$-17 \le h \le 17$, $-12 \le k \le 12$, $-13 \le l \le 13$
Reflections collected	10701
Independent reflections	2793[R (int) = 0.038]
Refinement method	Full-matrix least squares on F^2
Data/restraints/parameters	2793/3/144
Goodness-of-fit on F^2	1.02
Final R indices	R_1 = 0.0287
[$I > 2\sigma(I)$]	wR_2 = 0.0703
R indices (all data)	R_1 = 0.0362 wR_2 = 0.0736
Largest diff. Peak and hole (e $Å^{-3}$)	1.098/−0.443

3.4 | DFT computational analysis

3.4.1 | Molecular geometry

The ground state optimized the geometry of title compound was found to be almost consistent with the X-ray crystal structure results (Figure 4). Some experimental and computed values of the selected bond lengths, bond angles, and torsion angles for the title compound are listed in Table 4. It can be seen that the computed bond lengths are larger than the experimental values. However, this can be attributed to the neglect of intermolecular forces, such as van der Waals interactions and crystal packing forces in solid state, which make most of the experimental bond lengths to be shorter than the theoretical ones. Nevertheless, the root means square error between the experimental and computed values of bond lengths and bond angles is 8.7% and 1.8%, respectively, which indicates reasonable consistency. The calculated torsion angles C3-C4-C7-C8 and C5-C4-C7-N2 were 180.0°, while C3-C4-C7-N2 and C5-C4-C7-C8 were −180.0° and −0.0°, respectively, and the corresponding experimental torsion angles obtained from the X-ray structure analysis were 163.6(3)°, 169.6(2)°, −13.2(4)°, and 13.6(4)°, respectively. The torsion angle C3-C4-C7-C8 has the largest, and the torsion angle C5-C4-C7-C8 has the smallest discrepancy values of 16.4° and 10.4°, respectively.

TABLE 2 Hydrogen bond geometry (Å, °) for the title compound

D-H···A	D-H	H···A	D···A	D-H···A
N1-H1*A*···Br2^{i}	0.88	2.62	3.442 (2)	155
N1-H1*B*···Br2^{vi}	0.88	2.51	3.346 (3)	158
N2-H2*B*···O10^{v}	0.88	1.89	2.757 (3)	170
O10-H11···Br2^{vii}	0.83 (3)	2.54 (3)	3.353 (3)	164 (3)
O10-H12···Br2	0.83 (3)	2.51 (3)	3.309 (2)	161 (3)
C3-H3*A*···O1O^{v}	0.95	2.43	3.332(3)	158

Symmetry codes: (i) –x + 1, –y + 1, –z + 1; (v) –x + 1, y − 1/2, 1/2 − z; (vi) x–1,3/2–y, 1/2+ z; (vii) x, 3/2–y, z–1/2.

3.4.2 | Vibrational analysis

The vibrational analysis plays a significant role in determining conformational and structural features in the solid state. The vibrational spectrum of the investigated compound is given in Figure 5. For visual

TABLE 3 The selected interatomic distances (Å)

Br2···H1*A*^{i}	2.62	N2···H3*A*	2.64	H2*B*···H11^{v}	2.32
Br2···H1*B*^{ii}	2. 51	C3···H2*B*	2.70	H2*B*···H3*A*	2.14
Br2···H11^{iii}	2.54 (3)	C5···H8*A*	2.80	H2*B*···H12^{v}	2.44
Br2···H12	2.51 (3)	C8···H5*A*	2.70	H5*A*···H8*A*	2.24
O10···H3*A*^{iv}	2.43	H1*A*···H2*B*	2.47		
O10···H2*B*^{iv}	1.89	H2*A*···H6*A*^{v}	2.57		

Symmetry codes: (i) 1 − x, 1 − y, 1 − z; (ii) x + 1, 3/2 − y, z − 1/2; (iii) x, 3/2 − y, z + 1/2; (iv) 1 − x, 1/2 + y, 1/2 − z; (v) 1 − x, y − 1/2, 1/2 − z.

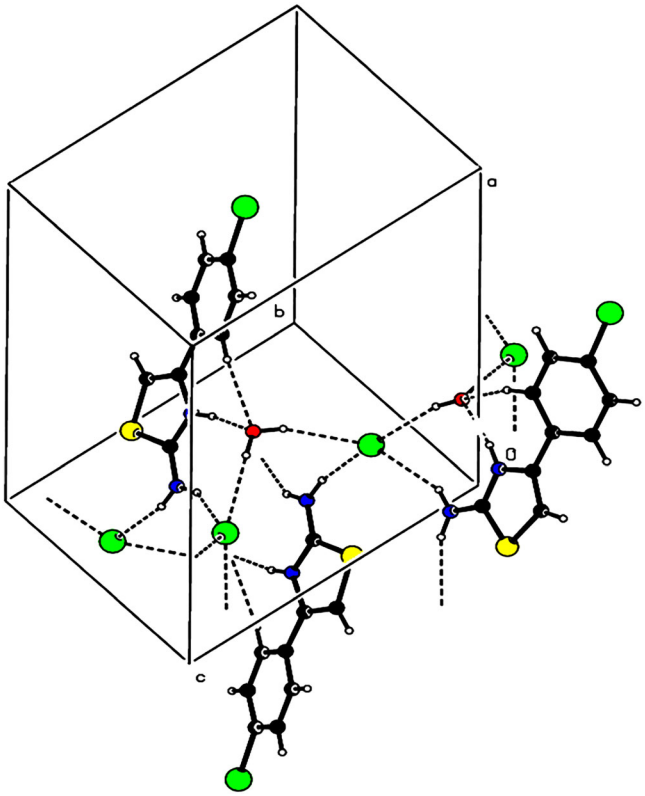

FIGURE 3 Part of the crystal structure. $N–H_{Thz}\cdots Br_{unccord}$, $N–H_{Thz}\cdots O_W$, $C–H\cdots O_W$, and $O_W–H_W\cdots Br_{unccord}$ (W = water, uncoord = uncoordinated and Thz = thiazole) hydrogen bonds are shown as dashed lines

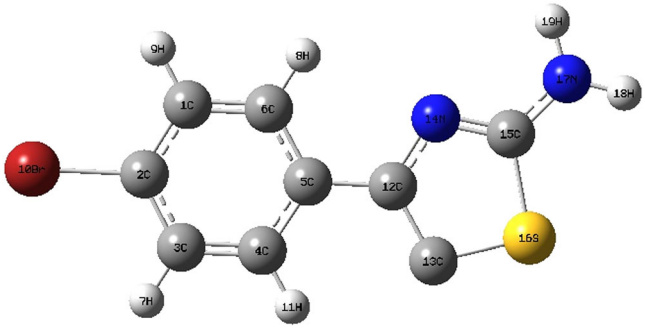

FIGURE 4 The optimized molecular structure of the title compound at B3LYP/6-311++G(d,p) level of theory

comparison, the simulated spectra computed at the DFT/B3LYP level using 6-311++G(d,p) basis set is also shown. Normally, the vibrational frequencies obtained by quantum chemical calculations with unscaled ab initio and DFT force field are greater than the experimental values due to anharmonicity and basis set deficiencies. In order to improve the agreement between calculated and the experimental values, it is necessary to scale down the calculated harmonic frequencies.[32] In the present study, a scaling factor of 0.978 was used to obtain a better agreement.[28]

In general, the assignment of C–S band in infrared is difficult, due to variable intensity band (1250-250 cm^{-1}). Moreover, C–S band is less polar compared with carbonyl group; as a consequence, it falls in lower frequency and weak band and it is also prone to coupling effects.[33] The absorption of the C–S group connected with other groups usually appears between 1250 and 1050 cm^{-1}. Considering these facts, the tentative assignment of the C–S group was assigned to bands at 1187 to 1040 cm^{-1}. The aromatic amines show C–N stretching absorptions in the region of 1382 to 1266 cm^{-1}.[34] In this study, the band at 1270 cm^{-1} was assigned to C–N absorption. The C=N band is observed at 1726 cm^{-1} in the FT-IR spectrum.

Usually, the N–H stretching vibrations occur in the region of 3500 to 3300 cm^{-1}. The asymmetric $–NH_2$ stretching vibration appears from 3500 to 3420 cm^{-1} and the symmetric, $–NH_2$ stretching is observed in the range of 3420 to 3340 cm^{-1}. In this study, the NH_2 asymmetric stretches were captured at 3410 cm^{-1} in the FT-IR spectrum. It was good agreement with HF and B3LYP/6-311++G(d,p) calculated values. Generally, C=C stretching vibrations occurred in the region of 1430 to 1650 cm^{-1}.[28,35] Accordingly, in the present study, the C=C stretching vibrations of 2-aminothiazole were assigned at 1356 and 1276 cm^{-1} in FT-IR. The ring stretching vibrations in FT-IR were assigned to 821 and 880 cm^{-1}. The experimental frequencies coincided with B3LYP/6-311++G(d,p) (DFT) frequencies results.

3.4.3 | HUMO-LUMO analysis

The energy gap between highest occupied molecular orbital (HOMO) and lowest unoccupied molecular orbital (LUMO) is quite helpful in determining electronic structures and is widely used in the analysis of chemical reactions.[36,38] According to Koopman theorem, ionization potential (IP), electron affinity (EA), and other reactivity parameters may be defined in terms of the energy of the HOMO and the LUMO.

The frontier molecular orbital energies were obtained using the B3LYP/6-311++G(d,p) level for the optimized molecular structure of the title compound. The three-dimensional plots of the frontier orbitals, the HOMO, and the LUMO along with HOMO−1 and LUMO+1 are shown in Table 5. The positive phase is shown in red colour, and the negative one is shown in green color. From the shapes of the orbitals, it is quite clear that the HOMO is localized over thiazole ring, while the LUMO is localized over phenyl ring, indicating an efficient electron transfer from thiazole group of the HOMO to the phenyl group of the LUMO if electronic transitions occur.

TABLE 4 Experimental and computed (B3LYP/6-311++G(d,p) geometric parameters of the title compound

	Bond Lengths, Å			Bond Angles, °			Torsion Angles, °	
Parameters	B3LYP	X-ray	Parameters	B3LYP	X-ray	Parameters	B3LYP	X-ray
Br1-C1	1.954	1.895(3)	C9-S1-C8	86.2	90.2(1)	C6-C1-C2-C3	−0.0	−1.2(5)
S1-C9	1.813	1.730(3)	C9-N2-C7	113.2	114.8(2)	Br1-C1-C2-C3	180.0	176.8(2)
S1-C8	1.848	1.731(3)	C2-C1-C6	120.9	120.7(3)	C1-C2-C3-C4	−0.0	−0.5(5)
N1-C9	1.409	1.323(3)	C2-C1-Br1	119.6	119.2(2)	C2-C3-C4-C5	0.0	1.9(4)
N2-C9	1.301	1.329(3)	C6-C1-Br1	119.5	120.1(2)	C2-C3-C4-C7	−180.0	−175.3(3)
N2-C7	1.361	1.406(3)	C3-C2-C1	119.4	119.4(3)	C3-C4-C5-C6	−0.0	−1.6(4)
C1-C2	1.391	1.386(4)	C2-C3-C4	121.0	121.1(3)	C7-C4-C5-C6	0.0	175.7(3)
C1-C6	1.393	1.388(4)	C3-C4-C5	118.2	118.0(3)	C4-C5-C6-C1	−0.0	0.0(4)
C2-C3	1.396	1.386(4)	C3-C4-C7	119.8	122.4(2)	C2-C1-C6-C5	−0.0	1.5(4)
C3-C4	1.406	1.400(4)	C5-C4-C7	122.0	119.6(2)	Br1-C1-C6-C5	−180.0	−176.5(2)
C4-C5	1.407	1.404(4)	C6-C5-C4	121.1	121.2(2)	C9-N2-C7-C8	0.0	0.1(3)
C4-C7	1.474	1.463(4)	C5-C6-C1	119.3	119.5(3)	C9-N2-C7-C4	180.0	177.4(2)
C5-C6	1.394	1.378(4)	C8-C7-N2	114.0	111.3(2)	C3-C4-C7-C8	180.0	163.6(3)
C7-C8	1.080	1.345(4)	C8-C7-C4	126.7	127.7(2)	C5-C4-C7-C8	−0.0	−13.6(4)
			N2-C7-C4	120.7	120.9(2)	C3-C4-C7-N2	−180.0	−13.2(4)
			C7-C8-S1	111.4	112.5(2)	C5-C4-C7-N2	180.0	169.6(2)
			N1-C9-N2	125.4	125.0(2)	N2-C7-C8-S1	0.0	0.6(3)
			N1-C9-S1	120.7	123.8(2)	C4-C7-C8-S1	−180.0	−176.4(2)
			N2-C9-S1	114.0	111.2(2)	C9-S1-C8-C7	0.0	−0.9(2)
						C7-N2-C9-N1	180.0	179.6(3)
						C7-N2-C9-S1	0.0	−0.8(3)
						C8-S1-C9-N1	−180.0	−179.5(3)
						C8-S1-C9-N2	0.0	1.0(2)

By analysing HOMO and LUMO energy values, the global chemical reactivity descriptors, ie, the chemical potential (μ), electronegativity (χ), hardness (η), softness (S), and electrophilicity index (ω) were obtained and incorporated in Table 6. Since a strong nucleophile is characterized by a lower value of chemical potential and electrophilicity index, the obtained values point towards the reactive nature of the title compound. The chemical potential (μ) was computed negative which indicated that this compound does not decompose spontaneously into the compounds from which it is made up of.[33] The small value of hardness (η) and a large value of softness (S) indicated that the system is polarizable, which was further confirmed by the large value of computed dipole moment.[33] These values together with small HOMO-LUMO gap (ΔE) and negative binding energy confirmed that the title compound is polarizable and reactive in nature, hence could bind with DNA.[34]

3.4.4 | Molecular electrostatic potential

The molecular electrostatic potential (MEP) plays a crucial role in understanding the chemical reactivity of any structure, molecular interactions, biophysical recognition, hydrogen bonding interactions, molecular cluster, and crystal behaviour. Moreover, it helps to predict the regioselectivity such as sites of nucleophilic and electrophilic attacks. In addition to this, it provides correlations between chemical reactivity and the partial charges, dipole moments, and electronegativity of a molecule.

The three-dimensional plot of the MEP of the crystal based on the title compound was obtained from the optimized molecular structure (Figure 6). It is clear from the figure that areas related to phenyl ring atoms are showing slightly positive electrostatic potential (yellow colour) and hydrogen atoms of $-NH_2$ attached to the thiazole moiety are representing the regions of sharply positive electrostatic potential (blue colour). The low

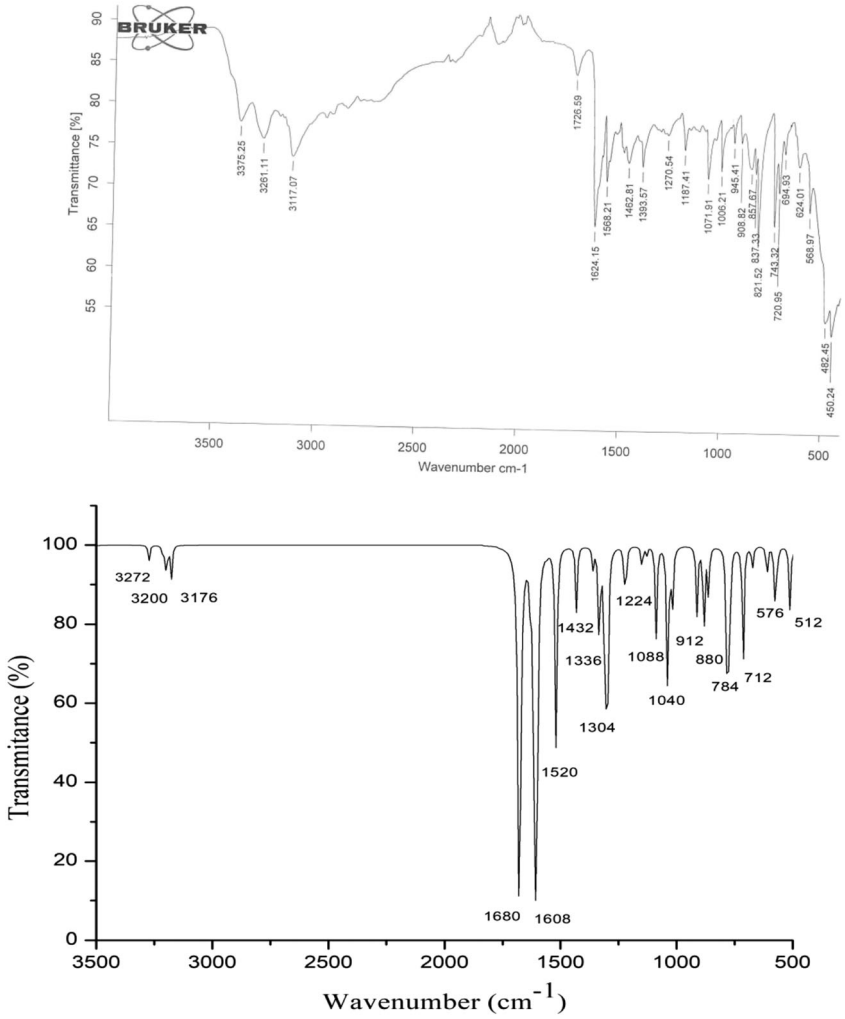

FIGURE 5 Experimental (top) and simulated [B3LYP/6-311++G(d,p)] (bottom) vibrational spectrum of the title compound

charge densities on the phenyl ring and hydrogen atoms of $-NH_2$ attached to thiazole moiety indicating the possible sites in the title compound for interactions via hydrogen bonding.

3.4.5 | Thermodynamic parameters

The thermodynamic data of a compound help in predicting and estimating the reactivity and feasibility of a chemical reaction. Furthermore, such data can be used to calculate many other inter-dependent thermodynamic parameters. The statistical thermo-chemical analysis of the title compound was carried out considering the molecule to be at standard temperature and pressure (298.15 K and 1 atm). The thermodynamic properties like heat capacity (Cp), enthalpy (H), Gibbs free energy (G), and entropy (S) were calculated using the DFT/B3LPY with 6-311G++(d,p) basis set. The thermodynamic quantities of the titled compound for various ranges (10-500 K) of temperatures were calculated using the Moltran software and the data is provided in Table S2. Most of the thermodynamics parameters have shown an increasing trend by increasing the temperature range from 10 to 500 K due to the fact that the vibrational intensities of the titled compound were changed with temperature.[39] The variations in H, S, and G with temperature were plotted and shown in Figure 7. Since increase in temperature increases the internal energy of the system, hence justified the rise in the values of H and S. Further, the contributions of S to G were found more at higher temperatures; the Gibbs free energy G values have shown a prominent decreasing trend at high temperatures.

3.5 | HS analysis

Visualization and exploration of intermolecular close contacts in the crystal structure of the title compound are invaluable. Thus, an HS analysis[40,41] was carried out by using Crystal Explorer 17.5 to investigate the locations of atoms···atom short contacts with potential to form hydrogen bonds and the quantitative ratios of these interactions besides of the π-stacking interactions. In the

TABLE 5 Molecular orbital surfaces and energy levels for the HOMO−1, HOMO, LUMO, and LUMO+1, of the title molecule

Type	LUMO	LUMO+1
	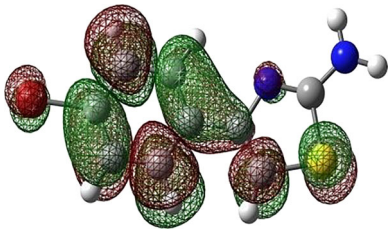	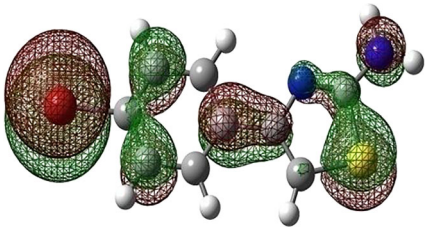
Energy	−0.16822 eV	−0.16527 eV
Type	**HOMO**	**HOMO−1**
	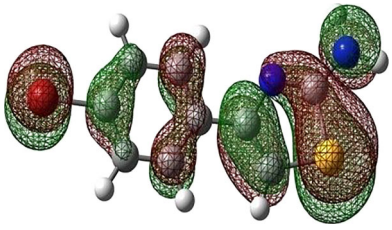	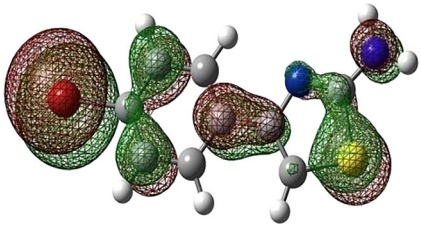
Energy	−0.26156 eV	−0.29478 eV

Abbreviations: HOMO, highest occupied molecular orbital; LUMO, lowest unoccupied molecular orbital.

TABLE 6 The calculated other parameters derived from HOMO-LUMO energy values

IP	0.26156	EA	0.16822
χ	0.21489	μ	−0.21489
η	0.04667	S	10.71
Ψ	0.49473	BE	−3425.52
D	7.1034		

Abbreviations: D, dipole moment (Debye); EA, electron affinity (eV); HOMO, highest occupied molecular orbital; IP, ionization potential (eV); LUMO, lowest unoccupied molecular orbital; χ, electronegativity; μ, chemical potential; ?, chemical hardness; S, chemical softness; Ψ, (electrophilicity index); BE, binding energy (hartrees).

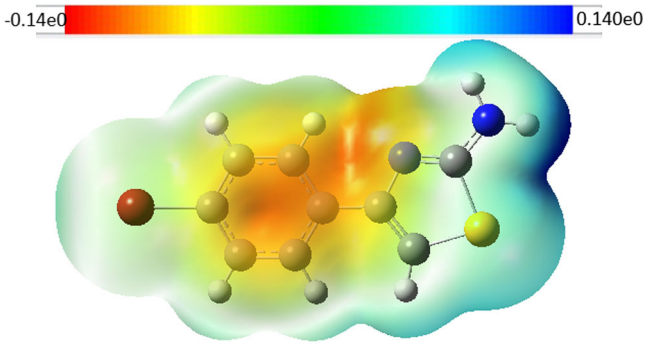

FIGURE 6 Molecular electrostatic potential (MEP) map of the title molecule calculated at B3LYP/6-311++G(d,p) level

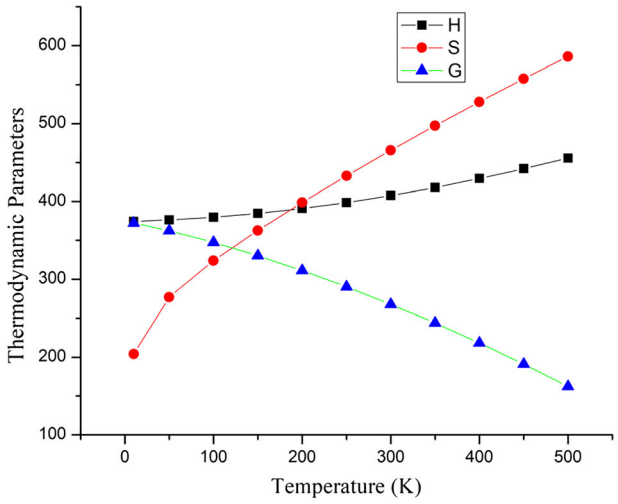

FIGURE 7 Effect of temperature on enthalpy, entropy, and Gibbs free energy values calculated by DFT method

HS plotted over d_{norm} (Figure 8), the white surface indicates contacts with distances equal to the sum of van der Waals radii, and the red and blue colours indicate distances shorter (in close contact) or longer (distinct contact) than the van der Waals radii, respectively.[42]

The bright-red spots appearing near uncoordinated Br2 and hydrogen atoms H1*A*, H1*B*, H2*B*, H11, H12, and H3*A* indicate their roles as the respective donors and acceptors in the dominant N–H···O, N–H···Br, O–H···Br, and C–H···O hydrogen bonds. The shape

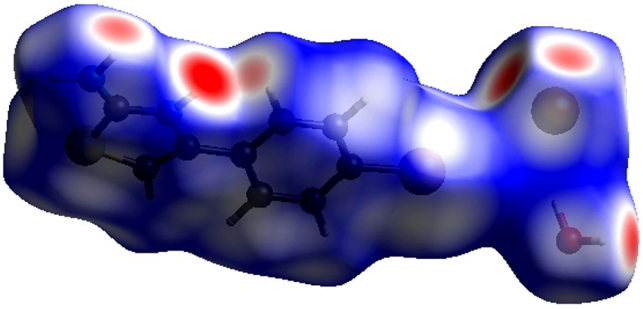

FIGURE 8 View of the three-dimensional Hirshfeld surface of the title compound plotted over d_{norm} in the range of −0.6597 to 1.0672 au

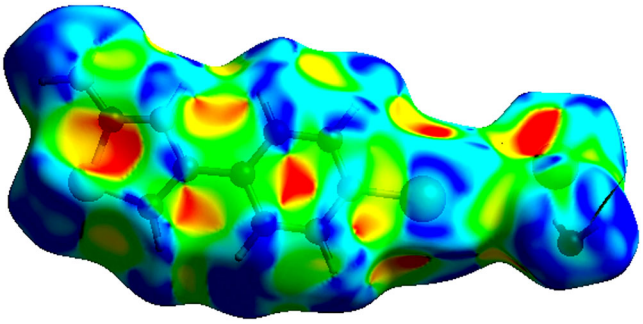

FIGURE 9 Hirshfeld surface of the title compound plotted over shape index

index of the HS is a tool to visualize the π···π stacking by the presence of adjacent red and blue triangles; if there are no adjacent red and/or blue triangles, then there are no π···π interactions. Figure 9 clearly suggest that there are π···π interactions in the title compound.

The overall two-dimensional fingerprint plot (Figure 10A) and those delineated into H···Br/Br···H, H···H, H···C/C···H, H···S/S···H, H···O/O···H, C···C, C···Br/Br···C, S···Br/Br···S, and N···C/C···N contact[43] are illustrated in Figure 10B-J, respectively, together with their relative contributions to the HS. The most important interaction is H···Br/Br···H contributing 30.4% to the overall crystal packing due to the interatomic H···Br contacts (Tables 3 and 4), which is reflected in Figure 10B as a pair of spikes with the tips at $d_e + d_i \sim 2.42$ Å. In the fingerprint plot delineated into H ···H contacts (Figure 10C), the 25.1% contribution to the HS is viewed as widely scattered points of high density due to the large hydrogen content of the molecule. The small single spike in the centre at $d_e = d_i = 1.2$ Å in Figure 10C is due to the short interatomic H···H contacts (Table 4). In the absence of C–H···π interactions in the crystal, the tiny pair of characteristic wings resulting in the fingerprint plot delineated into H···C/C···H contacts with 10.2% contribution to the HS (Figure 10D) and the pair of thin edges at $d_e + d_i \sim 3.36$ Å result from short interatomic H···C/C···H contacts. The H···S/S···H contacts in the structure with 8.3% contribution to the HS has an asymmetric distribution of points (Figure 10 E), with the tips at $d_e + d_i \sim 3.16$ Å. In the fingerprint plot delineated into H···O/O···H contacts (Figure 10F), the 7.5% contribution to the HS arises from the interatomic H···O/O···H contacts listed in Table 3 and is waived as a pair of spikes with the tips at $d_e + d_i \sim 1.77$ Å. The C ···C contacts assigned to short interatomic C···C contacts with 5.8% contribution to the HS appear as an arrow-shaped distribution of points in Figure 10G, with the vertex at $d_e = d_i \sim 1.70$ Å. The symmetrical distribution of points in the fingerprint plot delineated into C···Br/Br···C contacts (Figure 10H); the 4.0% contribution to the overall crystal packing is viewed as a pair of spikes with the tips at $d_e + d_i \sim 3.67$ Å. Finally, the S···Br/Br···S (Figure 10I) and N···C/C···N (Figure 10J) contacts in the structure with 2.6% and 2.1% contributions to the HS, respectively, have a nearly symmetric distribution of points, with the scattered points of low densities.

The HS representations with the function d_{norm} plotted onto the surface are shown for H···Br/Br···H, H···H, H···C/C···H, H···S/S···H, H···O/O···H, and C···C interactions in Figure 11A-F. The HS analysis confirms the importance of H-atom contacts in establishing the packing. The large number of H···Br/Br···H, H···H, H···C/C···H, H···S/S···H, and H···O/O···H interactions suggest that van der Waals interactions and hydrogen bonding play the major roles in the crystal packing.

3.6 | DNA binding studies

Reactivity and possible binding sites in the compound's structure as investigated by DFT were further explored experimentally for its binding with calf thymus (ct-) double strand (ds-) DNA by UV-visible spectroscopy and viscometry. Initially, spectroscopic experiments were run separately to obtain an individual spectrum of DNA and the test compound. DNA peak appeared at 260 nm, while for the test compound, a single peak appeared at 290.40 nm. Then, titrations were carried out by adding DNA in aliquots into fixed compound's concentration so that each addition gradually raised the DNA concentration into the reaction mixture from 10 to 60μM. Upon DNA additions, compound's peak shifted progressively towards shorter wavelength (blue shift) along with a gradual decrease in the absorbance maxima (Figure 12, left). The peak shifting was measured 5.2 nm from its initial position, which was quite significant to authenticate that the compound has interacted with DNA. The

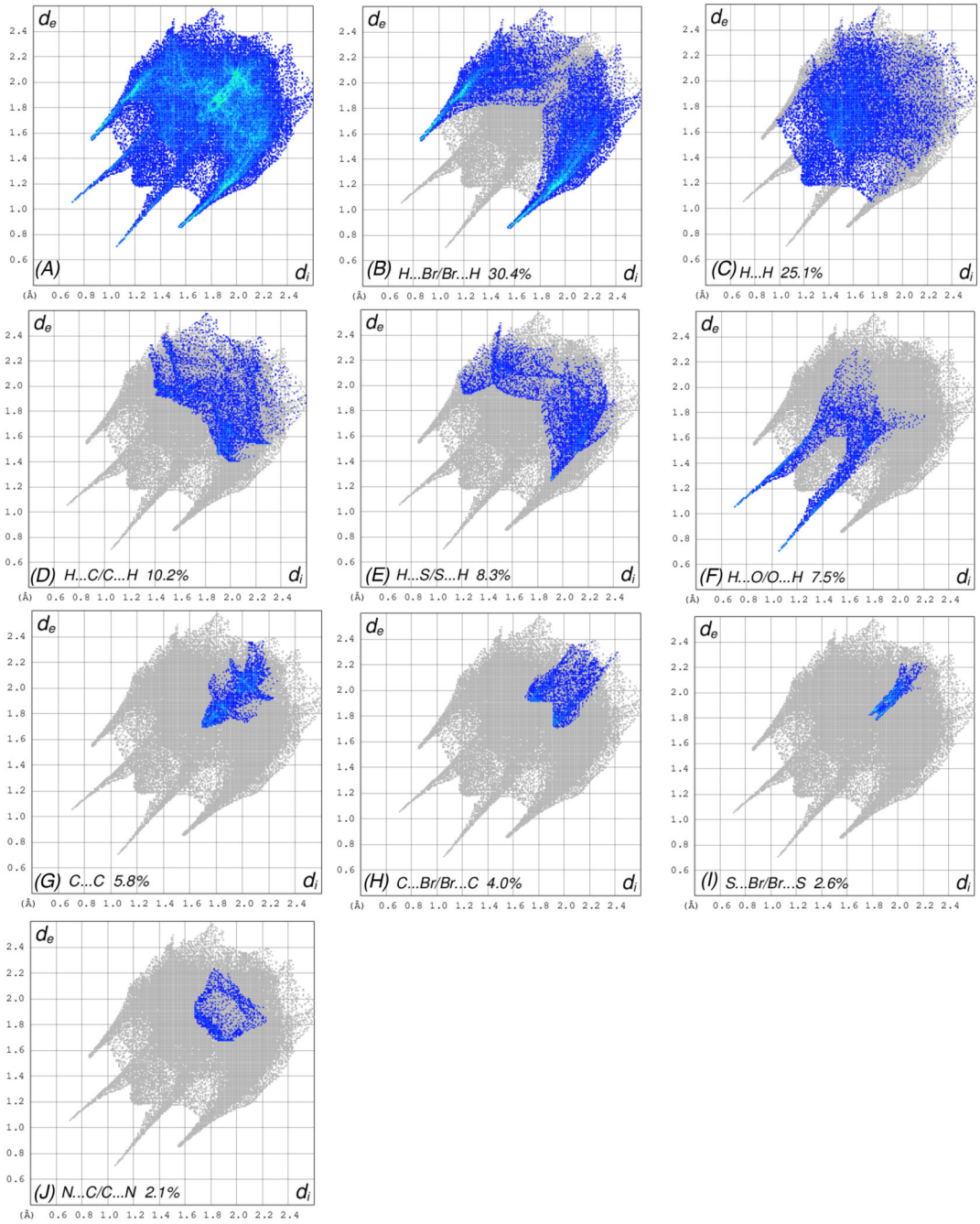

FIGURE 10 The full two-dimensional fingerprint plots for the title compound, showing A, all interactions, and delineated into B, H···Br/Br···H, C, H···H, D, H···C/C···H, E, H···S/S···H, F, H···O/O···H, G, C···C, H, C···Br/Br···C, I, S···Br/Br···S, and J, N···C/C···N interactions. The d_i and d_e values are the closest internal and external distances (in Å) from given points on the Hirshfeld surface contacts

observed hypochromism was evaluated as 23.24% by using Equation (1):

$$H\% = \frac{A_{free} - A_{bound}}{A_{free}} \times 100. \quad (1)$$

The binding possibility of the compound with DNA could further be explained on the bases of UV-spectral changes. The observed hypochromism and blue shift have been reported for intercalative binding of a compound with DNA.[44,45] Such binding possibility usually observed due to complete/or partial insertion of a compound into the DNA pocket and its chromophore's electronic state interact with DNA base pairs via overlapping; the coupling π orbital is partially filled by electrons and results in the reduction of transition

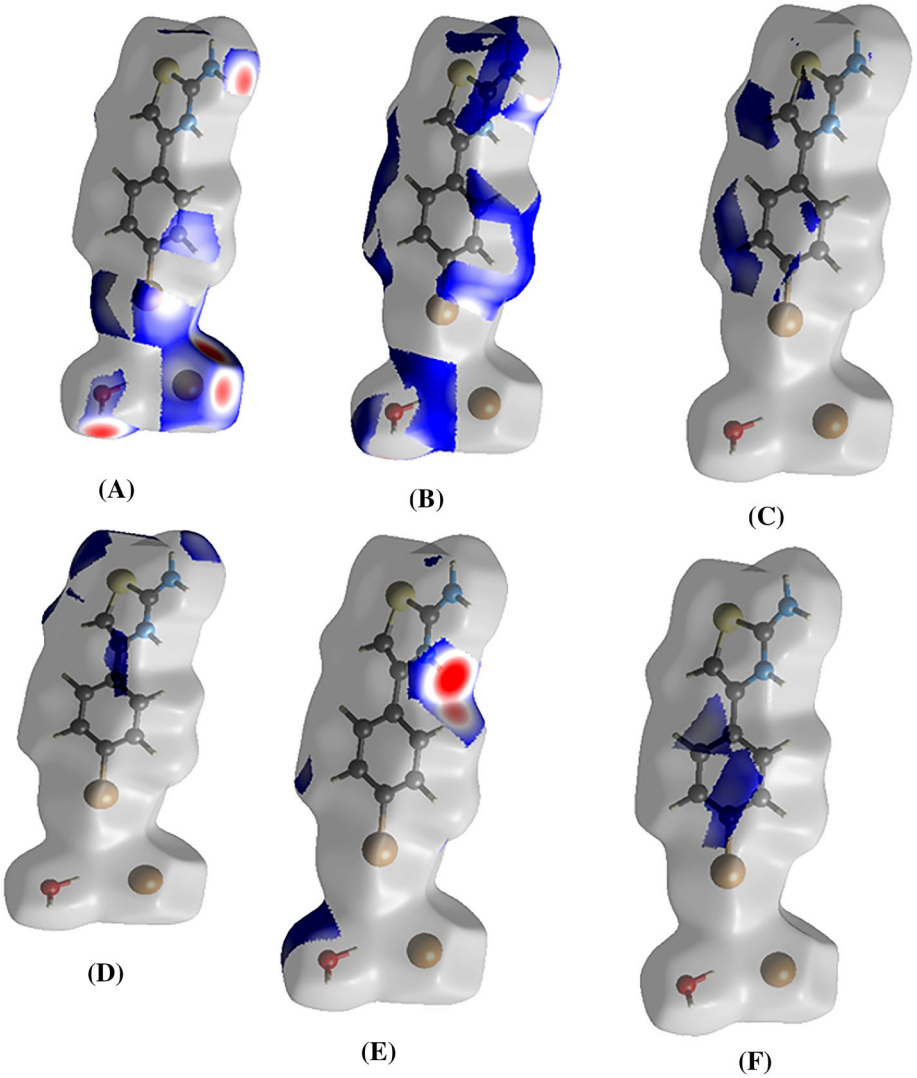

FIGURE 11 The Hirshfeld surface representations with the function d_{norm} plotted onto the surface for A, H···Br/Br···H, B, H···H, C, H···C/C···H, D, H···S/S···H, E, H···O/O···H, and F, C···C interactions

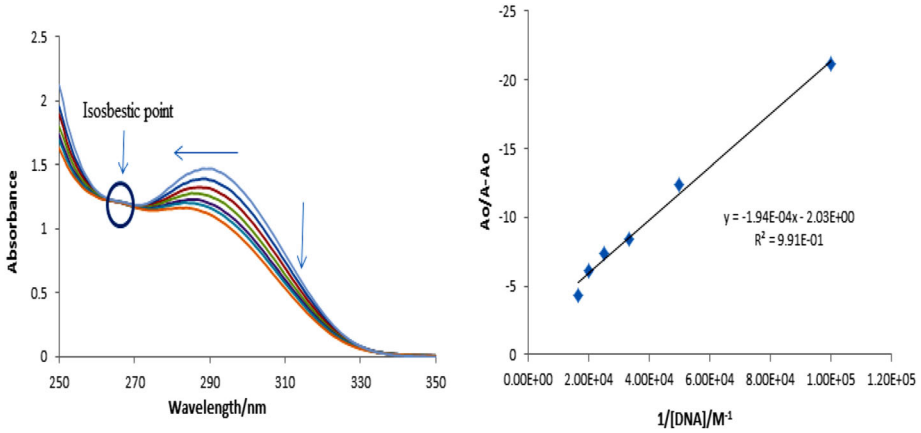

FIGURE 12 The UV-visible spectrum of the test compound on adding increasing concentrations of DNA (10 to 60μM) in a fixed concentration of compound (1.25×10^{-4}M) in (1:1) ethanol water at 37°C

probability (ie, hypchromism) of compound's chromophore after DNA addition.[41] The appearance of an isosbestic point in the UV spectra further suggested compound-DNA complex formation via intercalation and absence of other species except free and DNA bound complex.[46]

Intrinsic binding constant (K_b) and Gibbs free energy change (ΔG) for compound-DNA complex were calculated by using Benesi-Hildebrand and classical Vant Hoff equations (Equations 2 and 3, respectively).[44]

$$\frac{A_o}{A-A_o}=\frac{\varepsilon_G}{\varepsilon_{H-G}-\varepsilon_G}+\frac{\varepsilon_G}{\varepsilon_{H-G}-\varepsilon_G K_b[DNA]}, \quad (2)$$

$$\Delta G=-\mathrm{RT}\ \ln K_b \quad (3)$$

In Equation (2)), A_o and A are compound's absorption in the absence and presence of DNA, respectively; ε_G and ε_{H-G} are molar extinction coefficient of pure compound and compound-DNA complex, respectively. By plotting $A_o/A-A_o$ vs 1/[DNA], the value of binding constant, K_b, was obtained from the intercept to slope ratio (Figure 12, right). Binding constant was calculated to the value of $1.18 \times 10^4 M^{-1}$. The binding order (10^4) was evaluated greater than the reported intercalator isoxazocucumine ($6.3 \times 10^3 M^{-1}$) and more or less parallel to the values reported for typical intercalators lumazine ($1.74 \times 10^4 M^{-1}$), proflavine ($K = 2.32 \pm 0.41 \times 10^4 M^{-1}$), epirubicin ($K = 3.4 \times 10^4 M^{-1}$), anthracycline molecules ($K \approx 10^4$–$10^5 M^{-1}$), and other intercalators including methylene blue, acridine orange, and ethidium bromide ($K = 10^4 M^{-1}$ order for all).[47,48] K_b value of the test compound was further utilized in Equation (3), and ΔG were evaluated to the value of -24.16 kJ mol^{-1}, which showed spontaneity in the compound-DNA binding.

DNA binding by UV spectroscopy was further verified by measuring the viscosity of DNA in the presence of compound's concentrations. Viscosity measurements were made by adding 10 to 90μM compounds' concentration gradually into 1.45×10^{-5}M DNA solution. A plot was drawn between the cube root of relative specific viscosity and compound/DNA concentration ratio and is given in Figure 13. A linear rise in the relative viscosity of the DNA was observed until the additions of 60μM compound's concentrations into the DNA solution. After that, no significant change in the DNA viscosity was observed and seemed to be constant after 60μM additions of compound's concentration. This trend pointed towards a mixed mode of the compound-DNA binding and has been reported intercalative mode along with the possibility of minor groove binding.[49]

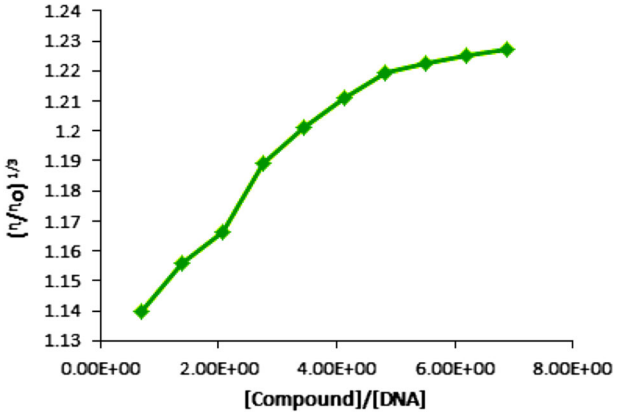

FIGURE 13 The plot of relative specific viscosity vs compound to DNA concentrations ratio, on adding increasing concentrations of the compound from 10 to 90 μM into 1.45×10^{-5}M DNA

4 | CONCLUSIONS

Gabriel cyclization reaction was employed to synthesize the title compound **4** using LR as an effective thionating reagent that provides high yield and the results are reproducible. The single crystal X-ray structure determination of the title compound confirmed the structural assignment from spectroscopic data. X-ray crystal analysis suggested dominant interactions in the crystal packing via hydrogen bonding and van der Waals contacts. HOMO-LUMO analysis by DFT revealed delocalization of electronic clouds over thiazole ring and the electronic transport properties from thiazole to phenyl ring. Theoretical studies on quantum parameters, vibrational analysis, and thermodynamic properties further provided detailed insights about the chemical reactivity, conformational details, and temperature effect. For the visualization and exploration of the intermolecular close contacts in the crystal structure of the title compound, a detailed HS analysis was carried out to investigate the locations of atoms···atom short contacts with potential to form hydrogen bonds and the quantitative ratios of these interactions besides of the π-stacking interactions. Spectroscopic and viscometric DNA binding studies revealed that the test compound has a potency to bind with DNA via intercalation. However, further work on this compound from biological and pharmaceutical aspects could help to explore it as a potential anticancer drug agent.

ACKNOWLEDGEMENTS

The authors would like to thank all the mentioned departments of national and international universities/institutes for the accomplishment of research explored in this paper.

CONFLICT OF INTEREST

Authors declare no conflict of interest.

ORCID

Nasima Arshad https://orcid.org/0000-0002-4257-9909

REFERENCES

[1] a) A. W. Hofmann, *Ber.* **1879**, *12*, 1126. b) A. W. Hofmann, *Ber.* **1880**, *13*, 8; c) A. Hantzsch, J. H. Weber, *Ber.* **1887**, *3118*, 3336.

[2] N. Siddiqui, M. F. Arshad, W. Ahsan, M. S. Alam, *Int. J. Pharm. Sci., Drug Res.* **2009**, *1*, 136.

[3] A. Dondoni, A. Marra, *Chem. Rev.* **2004**, *104*, 2557.

[4] N. A. A. Elkanzi, *J. Chin. Chem. Soc.* **2018**, *65*, 189.

[5] A. Saeed, P. A. Channar, G. Shabir, F. A. Larik, *J. Fluoresc.* **2006**, *26*, 1067.

[6] J. Das, P. Chen, D. Norris, R. Padmanabha, J. Lin, R. V. Moquin, Z. Shen, L. S. Cook, A. M. Doweyko, S. Pitt, S. Pang, *J. Med. Chem.* **2006**, *49*, 6819.

[7] M. V. N. D. Souza, M. V. D. Almeida, *Química Nova* **2003**, *26*, 366.

[8] A. C. Pasqualotto, K. O. Thiele, L. Z. Goldani, *Curr. Opin. Investig. Drugs* **2010**, *11*, 165.

[9] L. M. Fox, L. D. Saravolatz, *Clin. Infect. Dis.* **2005**, *40*, 1173.

[10] M. Zia-ur-Rehman, J. A. Choudary, S. Ahmad, *Bull. Korean Chem. Soc.* **2005**, *26*, 1771.

[11] M. P. Knadler, R. F. Bergstrom, J. T. Callaghan, A. L. A. N. Rubin, *Drug Metab. Dispos.* **1986**, *14*, 175.

[12] R. Nauen, U. Ebbinghaus-Kintscher, V. L. Salgado, M. Kaussmann, *Pestic. Biochem. Physiol.* **2003**, *76*, 55.

[13] A. J. Seed, P. Sampson, *Liq. Cryst.* **2017**, *44*, 1894.

[14] J. W. Goodby, R. J. Mandle, E. J. Davis, T. Zhong, S. J. Cowling, *Liq. Cryst.* **2015**, *42*, 593.

[15] V. Polshettiwar, M. P. Kaushik, *Liq. Cryst.* **2004**, *45*, 6255.

[16] T. J. Curphey, *J. Org. Chem.* **2002**, *67*, 6461.

[17] B. Böttcher, F. Bauer, *Eur. J. Org. Chem.* **1951**, *574*, 218.

[18] T. T. Nguyen, T. N. Le, P. E. Hansen, F. Duus, *Tetrahedron Lett.* **2006**, *47*, 8433.

[19] R. M. Elofson, L. A. Baker, F. F. Gadallah, R. A. Sikstrom, *J. Org. Chem.* **1964**, *29*, 1355.

[20] U. Pathak, L. K. Pandey, R. Tank, *J. Org. Chem.* **2008**, *73*, 2890.

[21] A. Degl'Innocenti, A. Capperucci, G. Mordini, G. Reginato, A. Ricci, F. Cerreta, *Tetrahedron Lett.* **1993**, *34*, 873.

[22] F. A. Larik, A. Saeed, U. Muqadar, P. A. Channar, *J. Sulphur Chem.* **2017**, *38*, 206.

[23] F. A. Larik, A. Saeed, U. Muqadar, H. El-Seedi, M. Faisal, P. A. Channar, H. Mehfooz, *Phosphorus, Sulfur Silicon Relat. Elem.* **2017**, *192*, 490.

[24] A. Saeed, H. Mehfooz, F. A. Larik, M. Faisal, P. A. Channar, *J. Asian Nat. Prod. Res.* **2017**, *19*, 1114.

[25] Bruker, SADABS, Bruker AXS Inc. Madison, Wisconsin, USA, **2009**.

[26] a) V. R. Hartwar, M. Sist, M. R. V. Jorgensen, A. H. Mamakhel, X. Wang, C. M. Hoffmann, K. Sugimoto, J. Overgaard, B. B. Iversen, *IUCr J.* **2015**, *2*, 563. b) G. M. Sheldrick, *ActaCryst.* **2008**, *64*, 112.

[27] M. J. Frisch, G. W. Trucks, H. B. Schlegel, G. E. Scuseria, M. A. Robb, J. R. Cheeseman, H. Nakatsuji, M. Caricato, X. Li, H. P. Hratchian, K. Toyota, R. Fukuda, J. Hasegawa, M. Ishida, R. Nakajima, Y. Honda, O. Kilao, H. Nakai, T. Verven, J. A. Montgomery Jr., J. E. Peralta, F. Ogliaro, M. Bearpark, J. J. Heyd, E. Brothers, K. N. Kudin, V.N. Staroveror, R. Kobayashi, J. Normand, K. Ragavachari, A. Rendell, J.C. Burant, S. J. Tomasi, M. Cossi, N. Rega, J. M. Millam, M. Klene, J. E. Knox, J. B. Cross, V. Bakken, C. Adamo, J. Jaramillo, R. Gomperts, R. E. Strattmann, O. Yazyev, A. J. Austin, R. Cammi, J. W. Ochetrski, R. L. Martin, K. Morokuma, V. G. Zakrazawski, G. A. Votn, P. Salvador, J. J. Dannenberg, S. Dapprich, A. D. Daniels, O. Farkas, J. B. Foresman, O. G. Gaussian, Revision A.O2, Gaussian Inc.,Wallingford, CT **2009**.

[28] Y. Erdogdu, D. Manimaran, M. T. Güllüo lu, M. Amalanathan, I. Hubert Joe, S. Yurdakul, *Opt. Spectrosc.* **2013**, *114*, 525.

[29] M. J. Turner, J. J. McKinnon, S. K. Wolff, D. J. Grimwood, P. R. Spackman, D. Jayatilaka, M. A. Spackman, *Cryt. Exp.* **2017**, 17.

[30] S. S. Babkina, N. A. Ulakhovich, *Anal. Chem.* **2005**, *77*, 5678.

[31] S. V. Giofre, R. Romeo, R. Mancuso, N. Cicero, N. Corriero, U. Chiacchio, G. Romeo, B. Gabriele, *RSC Adv.* **2016**, *6*, 20777.

[32] L. Legnani, L. Toma, P. Caramella, M.A. Chiacchio, S. Giofre, I. Delso, T. Tejero, P. Merino, *J. Org. Chem.* **2016**, *81*, 7733.

[33] A. Bendjeddou, T. Abbaz, S. Maache, A. Gouasmia, D. Villemin, *Int. J. Pharm. Sci. Rev. Res.* **2016**, *39*, 136.

[34] C. S. Abraham, J. C. Prasana, S. Muthu, M. Raja, *J. Mol. Struct.* **2018**, *1160*, 393.

[35] M. Karaback, M. Cinar, M. Kurt, *J. Mol. Struct.* **2008**, *885*, 28.

[36] R. J. Xavier, E. Gobinath, *Spectrochim. Acta A.* **2012**, *86*, 242.

[37] A. U. Rani, N. Sundaraganesan, M. Kurt, M. Cinar, M. Karabacak, *Spectrochim. Acta A.* **2010**, *75*, 1523.

[38] H. Gökce, S. Bahçeli, *Spectrochim. Acta A* **2013**, *114*, 61.

[39] V. Balachandran, G. Santhi, V. Karpagam, A. Lakshmi, *Spectrochim. Acta Part A: Mol. Biomol. Spectrosc.* **2013**, *110*, 130.

[40] F. L. Hirshfeld, *Theor. Chim. Acta* **1977**, *44*, 129.

[41] M. A. Spackman, D. Jayatilaka, *Cryst. Eng. Comm.* **2009**, *11*, 19.

[42] P. Venkatesan, S. Thamotharan, A. Ilangovan, H. Liang, T. Sundius, *Spectrochim. Acta A* **2016**, *153*, 625.

[43] J. J. McKinnon, D. Jayatilaka, M. A. Spackman, *Chem. Commun.* **2007**, *37*, 3814.

[44] N. Arshad, S. I. Farooq, M. H. Bhatti, S. Saleem, B. Mirza, *J. Photochem. Photobiol. B: Biol.* **2013**, *125*, 70.

[45] Z. Rehman, A. Shah, N. Muhammad, S. Ali, R. Qureshi, A. Meetsma, I. S. Butler, *Eur. J. Med. Chem.* **2009**, *44*, 3986.

[46] K. W. Kohn, M. J. Waring, D. Glaubiger, C. A. Friedman, *Cancer Res.* **1975**, *35*, 71.

[47] N. Arshad, M. H. Bhatti, S. I. Farooq, S. Saleem, B. Mirza, *Arab. J. Chem.* **2016**, *9*, 451.

[48] N. Arshad, M. Ahmad, M. Z. Ashraf, H. Nadeem, *J. Photochem. Photobiol B: Biol.* **2014**, *138*, 331.

[49] N. K. Janjua, A. Shaheen, A. Yaqub, F. Perveen, S. Sabahat, M. Mumtaz, C. Jacob, L. A. Ba, H. A. Mohammed, *Spectrochim. Acta Part A.* **2011**, *79*, 1600.

SUPPORTING INFORMATION

Additional supporting information may be found online in the Supporting Information section at the end of the article.

How to cite this article: Channar PA, Arshad N, Larik FA, et al. 4-(4-Bromophenyl)thiazol-2-amine: Crystal structure determination, DFT calculations, visualizing intermolecular interactions using Hirshfeld surface analysis, and DNA binding studies. *J Phys Org Chem*. 2019;e3968. https://doi.org/10.1002/poc.3968